International Journal of Theoretical and Applied Mathematics
2026, Vol. 12, No. 5, pp. 99–113
https://doi.org/10.11648/j.ijtam.20261205.12

SciencePG
Science Publishing Group

Research Article

LTNE Brinkman Convection of a Fluid Saturated Anisotropic Porous Layer with Temperature-dependent Internal Heat Generation

Sridhar Kulkarni [1,*], **Nagappa Kallappa Enagi** [2]

[1]Department of Mathematics, Government First Grade College, Paschapur, India
[2]Department of Mathematics, KRCE Society Arts and Science College, Bailhongal, India

Abstract

The study of anisotropic fluid-saturated porous convection is carried out by applying a local thermal non-equilibrium (LTNE) Brinkman model with temperature-dependent internal heat generation. The porous medium is assumed to be anisotropic. As the solid and fluid media are considered to have different temperatures, two field model energy equations are employed to describe their respective temperature fields. Temperature-dependent internal heat generation is considered in both phases,thereby introducing a tllermal feedback mechanism into tlle system. The Brinkman term is included in the momentum equation to account for viscous effects in tlle porous medium. The governing equations are linearized using the perturbation method and analyzed by normal mode analysis to obtain the stability characteristics and the critical conditions for the onset of convection. The effects of mechanical anisotropy, thermal anisotropy, thermal conductivity ratio, tllermal diffusivity ratio, interphase heat transfer, and temperature-dependent internal heat generation on the critical Rayleigh number and critical wave number are examined. The results demonstrate that tllese parameters significantly influence the stability of tlle system and modify the conditions required for the initiation of convection. The obtained results provide insight into tlle coupled effects of anisotropy, LTNE, Brinkman effects, and temperature-dependent internal heat generation in porous-media convection.

Keywords

Internal Heat, Porous Media, Heat Transfer, Convection, Porosity, LTNE Model, Stability

1. Introduction

Thermal convection in fluid-saturated porous layers has been an area of great interest because of its relevance to heat transfer and fluid transport in natural and engineering systems. Particular attention has been paid to the stability of a horizontal porous layer with a temperature distribution causing buoyancy-driven fluid motion. The conditions for the instability of a stationary conductive state in relation to convective flow are studied. The study of thermal convection in porous media has evolved from simple isotropic models to more realistic cases with anisotropic material properties. In many practical cases, the permeability and thermal conductivity of a porous structure are dependent on direction due to the internal architecture, the pore distribution, or preferential fiber alignment. These directional changes strongly influence the fluid motion, heat transfer and conditions for the onset of convective instability.

Banu and Rees [1] employed the LTNE model to investigate heat transfer and convective instability in porous media by considering the thermal interaction between the fluid and solid

*Correspondence: Sridhar Kulkarni (kulkarnidrsridhar11@gmail.com)

Received: 10 October 2026; **Accepted:** 22 October 2026; **Published:** 23 November 2026

Copyright: © The Author(s), 2026. Published by Science Publishing Group. This is an **Open Access** article, distributed under the terms of the Creative Commons Attribution 4.0 License (http://creativecommons.org/licenses/by/4.0/), which permits unrestricted use, distribution and reproduction in any medium, provided the original work is properly cited.

phases. Their analysis demonstrated that the LTNE parameters significantly influence the critical Rayleigh number and critical wave number associated with the onset of convection. Govender [2] investigated the influence of thermal anisotropy on the stability of convection in rotating porous media and reported that an increase in the thermal anisotropy ratio stabilizes the system. Malashetty et al. [3, 4] examined the influence of thermal non-equilibrium on the onset of convection in a densely packed porous layer by considering anisotropy in permeability and thermal diffusivity. Subsequently, Postelnicu [5] analyzed the influence of inertia on the onset of mixed convection in a porous layer and showed that inertia has a stabilizing influence on the onset of convection. The study further indicated that the stabilizing effect of inertia can dominate the influence of local thermal non-equilibrium conditions. Shivakumara and Mamatha [6] investigated the influence of anisotropy on heat transfer and convective instability in porous media under LTNE conditions. Their analysis demonstrated that anisotropy can substantially modify the thermal characteristics and stability behaviour of the porous system. Mahajan and Nandal [7] examined anisotropic penetrative convection in a porous layer under LTNE conditions while incorporating Brinkman effects. They showed that anisotropy and thermal non-equilibrium substantially affect the stability characteristics and that internal heat generation can promote the possibility of subcritical instability. Storesletten and Rees [8] examined the onset of convection in an inclined anisotropic porous layer with internal heat generation. They reported that the preferred mode of motion at the onset of convection depends strongly on both the anisotropy ratio and the angle of inclination. The nonlinear stability characteristics of LTNE convection have also been investigated. Straughan [9] examined global nonlinear stability in porous convection using a thermal non-equilibrium model and found that the global nonlinear stability threshold coincides with the linear instability threshold. This result provides an important connection between linear and nonlinear stability analyses of convection in LTNE porous systems. Nandal [10] investigated the combined influence of internal heat generation and heat extraction on the onset of anisotropic Darcy–Brinkman penetrative convection under LTNE conditions. The study indicated that internal heat generation within the fluid phase can promote the occurrence of subcritical instability. More recently, Bixapathi and Babu [11] investigated the effect of internal heat modulation on convective instability in a porous layer subjected to a magnetic field using the Brinkman model. Their results indicated that internal heating, magnetic field strength, and Brinkman effects can delay the onset of stationary convection, thereby exerting a stabilizing influence on the system.

Enagi et al. [12] examined the combined effects of internal heat generation and the density maximum on the onset of convection in a couple-stress fluid-saturated porous layer. They reported that internal heat generation, conductivity ratio, and the density function can significantly influence the stability characteristics and, under the considered conditions, have a destabilizing effect on the onset of convection. Mahantesh et al. [13] investigated heat transfer in an anisotropic porous layer by considering directional variations in the relevant physical properties together with internal heat generation. Their results demonstrated that both anisotropy and internal heat generation can substantially modify the heat-transfer characteristics and stability behaviour. Praveena et al. [14] studied the influence of internal heating on the stability of thermal convection in a couple-stress fluid-saturated porous slab. Their analysis showed that the physical properties of the fluid and the magnitude of internal heat generation play important roles in determining the convective behaviour of the system. Nouri-Borujerdi et al. [15] investigated the influence of uniform internal heat generation on convective instability in a horizontal channel filled with porous material. Their results highlighted the importance of internal heat sources in modifying the thermal and hydrodynamic characteristics of porous systems. Honnappa [16] investigated oscillatory convection in an Oldroyd-B fluid-saturated porous layer in the presence of variable gravity and temperature-dependent internal heating. The results showed that both temperature-dependent internal heat generation and variable gravity can delay the onset of convection and thereby stabilize the system under the conditions considered. Early contributions by Castinel and Combarnous [17] demonstrated the importance of directional permeability in the onset of convection in horizontal porous layers. Epherre [18] then investigated the influence of anisotropic thermal diffusivity. The conceptual foundations and subsequent developments of this field are thoroughly discussed by Ingham and Pop [19]. The contributions represent a major basis for the understanding of the mechanisms governing the convective onset and for the extension of the classical stability analyzes to more complex porous-media configurations. Later, the effect of mechanical and thermal anisotropy, vertical throughflow, and internal heat generation on convective instability was studied by Khalili et al. [20]. The classical analysis of convection in saturated porous media is generally based on the assumption of local thermal equilibrium (LTE), i.e., the fluid and the solid matrix are at the same temperature at all points. This approximation may not be valid when the heat exchange between the two phases is not sufficient to establish thermal equilibrium. For a review of the development of nonequilibrium models and their application to porous-medium convection, see Kuznetsov [21]. Kvernvold and Tyvand [22] extended the theoretical knowledge on convec-

tive behavior in anisotropic porous structures. Review articles that discuss the broader significance of these developments include McKibbin [23]. Nield and Bejan [24] discussed the fundamental mechanisms of convection in porous media and the development of theoretical models for understanding convective instability.Nilsen and Storesletten [25] gave an analytical study of natural convection in rectangular porous channels. The effects of anisotropic permeability based on the Brinkman momentum equation, which goes beyond the classical Darcy formulation, were investigated by Qin and Kaloni [26]. To overcome the limitations of the LTE model, the local thermal non-equilibrium (LTNE) approach separates the temperatures of the fluid and solid phases, and describes their thermal interaction using separate energy equations coupled via an interphase heat transport term. The development and application of this two-equation model for heat transfer in porous media were presented by Rees & Pop [27–29]. The LTNE framework thus provides a more complete basis to study convective instability in situations where the thermal responses of the fluid and the solid phases are different.The effects of anisotropy on convective flow through porous media were discussed by Storesletten [30]. Tyvand and Storesletten [31] studied convection in layers with principal anisotropy directions inclined relative to gravity.The broader developments and applications of porous-media transport phenomena are also discussed by Vafai [32].

These studies collectively demonstrate the importance of the directional dependence of porous-medium properties for understanding convective stability, and provide the basis for future work involving more complex heat-transfer mechanisms.Internal heat generation has received considerable attention because it can significantly modify the thermal field and consequently alter the stability characteristics of porous layers.

The study of thermal convection in fluid-saturated porous media is of great importance for many engineering and environmental applications such as geothermal energy extraction, thermal insulation, packed-bed reactors, porous heat exchangers, and underground heat transport. Such systems are affected by different temperature differences that can drive buoyancy-driven fluid motion, which in turn influences heat-transfer rates and thermal stability. The onset and structure of convective motion can be further modified by the directional dependence of permeability and thermal conductivity in anisotropic porous materials. Moreover, the local thermal non-equilibrium (LTNE) model can be used to describe the heat transfer between the two phases more realistically when the solid matrix and the saturating fluid are at different temperatures. The internal heat generation also affects the temperature field and the stability characteristics of the system. Thus, the study of the onset of convection in anisotropic porous layers with temperature-dependent internal heat generation under LTNE conditions is significant to understand the coupled effects of material anisotropy, interphase heat transfer, and thermal feedback on convective instability.

2. Mathematical Formulation

The present study investigates the onset of convection in an anisotropic porous layer with temperature-dependent internal heat generation using the local thermal non-equilibrium (LTNE) model. The analysis incorporates mechanical anisotropy, separate thermal anisotropy parameters for the fluid and solid phases, interphase heat transfer, and temperature-dependent internal heat generation.

The porous layer has a height h, and the fluid and solid phases are assumed to be in local thermal non-equilibrium, requiring separate energy equations for each phase. Furthermore, the internal heat generation is assumed to depend on temperature rather than being constant. The lower boundary is maintained at a higher temperature, while the upper boundary is maintained at a lower temperature. Let T_l and T_u denote the temperatures at the lower and upper boundaries, respectively. The governing equations are given as follows.

$$\nabla \cdot \vec{V} = 0 \tag{1}$$

$$\frac{\rho}{\varepsilon}\frac{\partial \vec{V}}{\partial t} + \nabla p - \rho\vec{g} + \frac{\mu}{K}\vec{V} = \mu_e \nabla^2 \vec{V} \tag{2}$$

$$\varepsilon(\rho_0 c)_f \frac{\partial T_f}{\partial t} + (\rho_0 c)_f (\vec{V}\cdot\nabla)T_f = \varepsilon k_{fx}\nabla^2 T_f + n(T_s - T_f) + \xi q_f (T_f - T_0) \tag{3}$$

$$(1-\varepsilon)(\rho_0 c)_s \frac{\partial T_s}{\partial t} = (1-\varepsilon)k_s \nabla^2 T_s - H(T_s - T_f) + (1-\varepsilon)q_s(T_s - T_u) \tag{4}$$

$$\rho = \rho_0 \left[1 - \beta(T_f - T_u)\right] \tag{5}$$

To eliminate the pressure term from equation (2) and create dimensionless expressions (3) to (5), apply the following transformations.

$$\begin{aligned} (x, y, z) &= h(x^*, y^*, z^*), \\ (u, v, w) &= \frac{\varepsilon k_f}{h(\rho_0 c)_f}(u^*, v^*, w^*), \\ p &= \frac{k_f \mu}{(\rho_0 c)_f K} p^*, \\ T_f &= (T_\ell - T_u)T_f^* + T_u, \\ T_s &= (T_\ell - T_u)T_s^* + T_u, \\ t &= \frac{(\rho_0 c)_f h^2}{k_f} t^* \end{aligned} \tag{6}$$

to obtain

$$\left(\frac{1}{Pr_D}\frac{\partial \vec{V}}{\partial t} + \nabla p - R_L T_f \vec{e}_z\right) = -\vec{V} + Da\nabla^4 \vec{V} \tag{7}$$

$$\frac{\partial T_f}{\partial t} + (\vec{V}\cdot\nabla)T_f = \eta_f \nabla_1^2 T_f + \frac{\partial^2 T_f}{\partial z^2} + N(T_s - T_f) + Q_f(T_f) \tag{8}$$

$$\alpha\frac{\partial T_s}{\partial t} = \eta_s \nabla_1^2 T_s + \frac{\partial^2 T_s}{\partial z^2} - \gamma N(T_s - T_f) + Q_s(T_s) \tag{9}$$

$$\alpha = \frac{(\rho_0 c)_s k_{fz}}{(\rho_0 c)_f k_{sz}}, \qquad R_L = \frac{\rho\beta g(T_\ell - T_u)hK}{\varepsilon\mu_f\kappa_f} \tag{10}$$

$$Da = \frac{\mu_e K}{\mu d^2}, \qquad H = \frac{nh^2}{\varepsilon k_{fz}}, \qquad \gamma = \frac{\varepsilon k_f}{(1-\varepsilon)k_s} \tag{11}$$

$$\eta_f = \frac{k_{fx}}{k_{fz}}, \qquad \eta_s = \frac{k_{sx}}{k_{sz}}, \qquad \xi = \frac{k_x}{k_z} \tag{12}$$

$$Pr_D = \frac{\nu h^2}{\varepsilon k_f K}, \qquad Q_f = \frac{q_f h^2}{\kappa_f}, \qquad Q_s = \frac{q_s h^2}{\kappa_f} \tag{13}$$

2.1. Basic State

It is presumed that the fundamental state is dormant and hence

$$u = v = w = 0, \qquad T_f = T_{fb}(z), \qquad T_s = T_{sb}(z) \tag{14}$$

The temperatures of the fluid and solid medium satisfy the basic state

$$\frac{d^2 T_{fb}}{dz^2} = 0 \tag{15}$$

$$\frac{d^2 T_{sb}}{dz^2} = 0 \tag{16}$$

with the boundary conditions,

$$\begin{aligned} T_{fb} = T_{sb} = 1 \quad &\text{at } z = 0, \\ T_{fb} = T_{sb} = 0 \quad &\text{at } z = 1 \end{aligned} \tag{17}$$

The basic state solutions satisfying the conditions (17) are

$$T_{fb} = T_{sb} = 1 - z \tag{18}$$

2.2. Perturbed State

As there are small disturbances in the basic state, the temperature and the velocity components under the perturbed state are given by

$$\begin{aligned} (u, v, w) &= (\widetilde{u}, \widetilde{v}, \widetilde{w}), \\ T_f = T_{fb} + \theta, \qquad T_s &= T_{sb} + \phi \end{aligned} \tag{19}$$

Substituting (19) into (7)–(9) with the basic state result, we get the perturbed expressions,

$$\frac{1}{Pr_D}\frac{\partial}{\partial t}(\nabla^2\widetilde{w}) - R_L\nabla_1^2\theta = -\frac{1}{\xi}\frac{\partial^2\widetilde{w}}{\partial z^2} + \nabla_1^2\widetilde{w} + Da\nabla^4\widetilde{w} \tag{20}$$

$$\frac{\partial\theta}{\partial t} - \widetilde{w} = \eta_f\nabla_1^2\theta + \frac{\partial^2\theta}{\partial z^2} + H(\phi - \theta) + Q_f\theta \tag{21}$$

$$\alpha\frac{\partial\phi}{\partial t} = \eta_s\nabla_1^2\phi + \frac{\partial^2\phi}{\partial z^2} - \gamma H(\phi - \theta) - Q_s\phi \tag{22}$$

The linearized forms of equations (20)–(22) are used to investigate the linear stability of the system subject to the boundary conditions (23). The normal-mode representation is introduced as follows:

$$\begin{aligned} \widetilde{w} = \frac{\partial^2\widetilde{w}}{\partial z^2} = 0 \quad &\text{at } z = 0, 1, \\ \theta = \phi = 0 \quad &\text{at } z = 0, 1 \end{aligned} \tag{23}$$

2.3. Linear Stability Analysis

The linearized forms of equations (20)–(22) are used to investigate the linear stability of the system subject to the boundary conditions (23). The normal-mode representation is taken as

$$[\widetilde{w}, \theta, \phi] = [W(z), \varphi(z), \phi(z)]\exp\{i(lx + my) + \omega t\}. \tag{24}$$

The horizontal wave number is defined by

$$a = \sqrt{l^2 + m^2},$$

and the differential operator is defined as

$$D = \frac{d}{dz}.$$

Here, a is the horizontal wave number, while ω denotes the temporal growth rate of the disturbance, assumed to be real. Substituting the normal-mode representation (24) into equations (17)–(19), we obtain

$$\left(\frac{D^2}{\xi} - a^2\right)W - Da\left(D^2 - a^2\right)^2 W - R_a a^2\varphi = 0 \tag{25}$$

$$(D^2 - a^2\eta_f)\varphi - W + H(W - \varphi) + Q_f\varphi = 0 \tag{26}$$

$$(D^2 - a^2\eta_s)W - \gamma H(W - \varphi) - Q_s W = 0 \tag{27}$$

The boundary conditions become

$$W = D^2 W = 0 \qquad \text{at } z = 0, 1. \tag{28}$$

To solve the resulting system using the one-term Galerkin method, we choose the following trial functions:

$$W = A\sin(\pi z), \varphi \quad = B\sin(\pi z), \phi = C\sin(\pi z). \tag{29}$$

Where

$$\delta^2 = a^2 + \pi^2,$$

and

$$B_1 = \pi^2 + a^2\xi, B_2 \quad = -\pi^2 - a^2\eta_f, B_3 = -\pi^2 - a^2\eta_s.$$

Since (29) satisfy the boundary conditions (28) therefore substitute (29) in the equations (25)-(27) we get the following matrix.

$$\begin{bmatrix} Da\delta^4 + B_1 & -R_L a^2\xi & 0 \\ 1 & B_2 - H & H - Q_f \\ 0 & \gamma H - Q_s & B_3 - \gamma H \end{bmatrix} \begin{bmatrix} A \\ B \\ C \end{bmatrix} = \begin{bmatrix} 0 \\ 0 \\ 0 \end{bmatrix}. \tag{30}$$

Equating the determinant of the above coefficient matrix to zero, we obtain the Rayleigh number R_a as follows

$$R_a = -\frac{(Da\,\delta^4 + B_1)}{a^2\xi}\left[(B_2 - H)(B_3 - H\gamma) - \frac{(H - q_f)(\gamma H - q_s)}{B_3 - \gamma H}\right]. \tag{31}$$

When $\eta_f = \eta_s = \xi = 0$ and $Da = 0$, the above equation (31) reduces to

$$R_a = -\frac{(\pi^2 + a^2)^2}{a^2}\left[1 - \frac{H}{(\pi^2 + a^2)^2\gamma H}\right].$$

This is the expression for the Rayleigh number given by Banu and Rees (2002) for the isotropic thermal non-equilibrium case.

3. Results and Discussion

Figure 1 depicts the variation of the Rayleigh number Ra with the wave number a for different values of the fluid phase internal heat generation parameter (Qf). From the figure, we observe that each curve is parabolic in nature and has a well-defined minimum point. This minimum point on each curve gives a value, which is called the critical Rayleigh number, Ra, and corresponding to this minimum Ra, there corresponds a minimum value of wave number, which is called the critical wave number. This number will define the stability criteria of the system. In the graph, for very small wave numbers, there is a need for a larger Rayleigh number to begin the instability of the system, as the corresponding convective cells are larger and less effective in heat transfer. When the wave number gradually increases, the Rayleigh number decreases, which means that smaller convection cells cause enhanced heat transfer efficiency. When the curves reach a minimum value, we observe that a further increase in wave number results in a rise in Ra, because the viscous and thermal diffusion effects start dominating the convective cells. It is also observed that, as the internal heat generation Qf increases, the neutral stability curves move upward, which means that the critical Rayleigh number increases with an increase in internal heat generation, indicating that more heat generated inside the fluid stabilizes the system and delays the start of the convection. This phenomenon is because heat generated inside the fluid increases the local temperature in the medium, and thus the difference in temperature between the boundaries decreases, thereby making buoyancy forces weak. Weak buoyancy makes it hard for convection to start, as these forces are crucial for its onset. Thus, the internal heat generation can influence the stability of a system and the conditions for the onset of convection. For smaller values of Qf (e.g., 0.0001, 0.005, 0.03), the position of the curves appears lower on the graph, which indicates that the system becomes unstable at a smaller Rayleigh number and thus the convection sets in earlier. On the other hand, as the fluid phase internal heat generation parameter Qf takes higher values, the minimum Rayleigh number increases, indicating greater stability. Moreover, at higher wave numbers, the effect of Qf is less pronounced because viscous dissipation dominates.

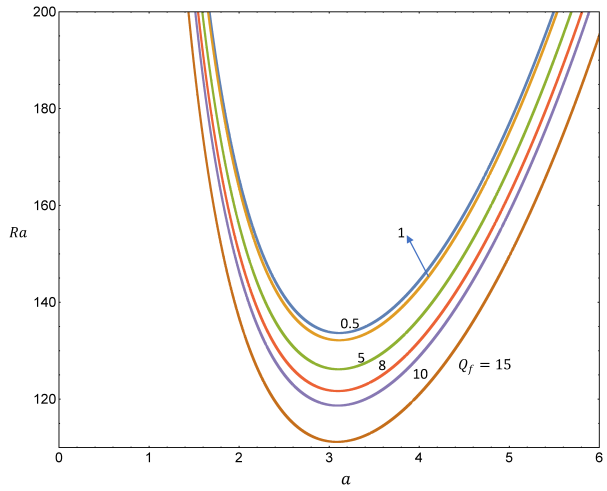


Figure 1. *Variation of Ra with wave number for different values of Qf.*

Figure 2 displays the dependence of the Rayleigh number on the wave number for several values of the solid phase internal heat generation parameter Qs. We observe in this figure that as the internal heat generation increases, the curves shift down a bit, meaning the critical Rayleigh number decreases. This tendency indicates that the greater internal heat generation in the solid phase enhances the local temperature gradient in the medium and, consequently, stronger buoyancy forces that lead to an earlier onset of convection. It is also worth mentioning that the internal heat produced is a destabilizing factor, lowering the thermal energy threshold for the onset of convection. However, at higher wave numbers, all the curves converge to a common limit, showing that the effect of internal heat generation becomes less important. This means that for larger wave numbers, the effect of internal heat generation is lessened as the conductive and viscous effects are dominant.

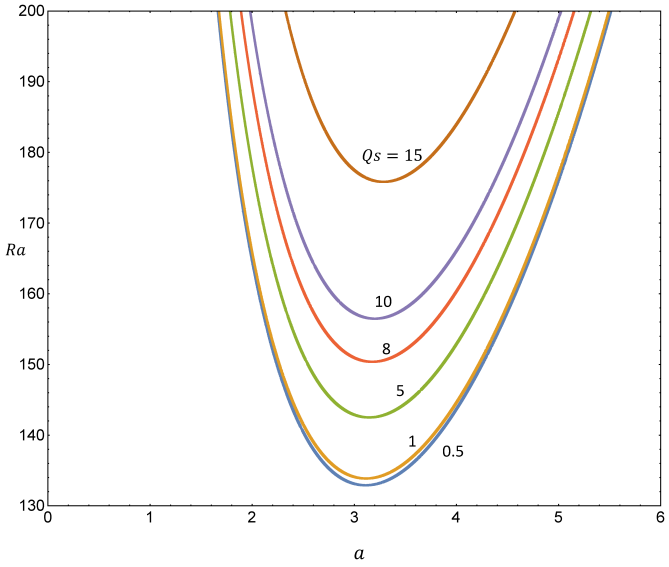


Figure 2. *Variation of Ra with wave number for different values of Qs.*

Figure 3 illustrates the variation of the neutral stability curves with the wave number for different values of the solid-phase thermal anisotropy parameter, ns. The effect of solid-phase thermal anisotropy is found to be similar to that of the fluid-phase internal heat generation parameter explained in Figure 1.

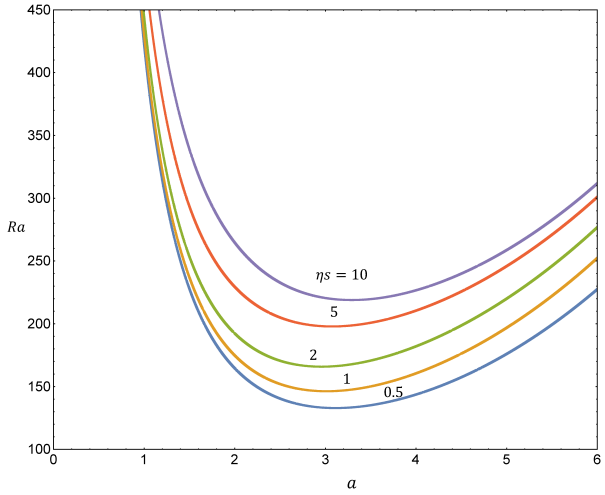


Figure 3. *Variation of Ra with wave number for different values of ηs.*

Figure 4 illustrates the variation of the neutral stability curves with the wave number for different values of the fluid-phase thermal anisotropy parameter, nf. It is observed that an increase in the fluid-phase thermal anisotropy parameter leads to an increase in the minimum Rayleigh number. This indicates that a greater thermal driving force is required to initiate convective motion, thereby exerting a stabilizing influence on the system. However, overall, Figure 4 highlights that the effect of the fluid-phase thermal anisotropy parameter is to make the system more stable.

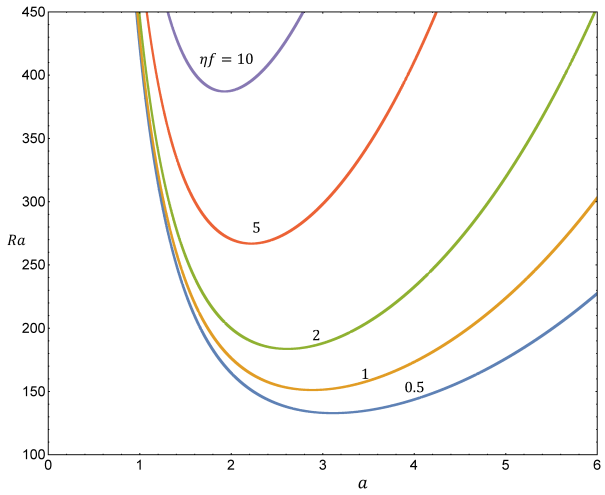


Figure 4. *Variation of Ra with wave number for different values of ηf.*

Figure 5 presents the variation of neutral stability curves with wave number for different values of the mechanical anisotropy parameter ξ. In this case, the effect of ξ is found to be similar to

that of the solid-phase internal heat generation parameter given in Figure 2. Overall, the mechanical anisotropy parameter has a destabilizing effect on the system.

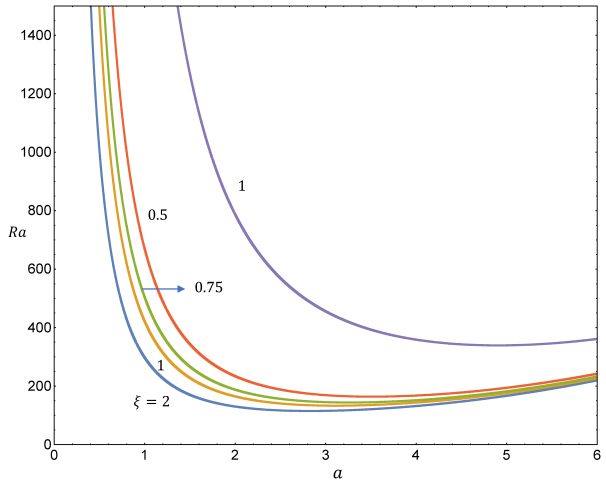


Figure 5. *Variation of Ra with wave number for different values of ξ.*

Figure 6 illustrates the variation of the neutral stability curves with the wave number for different values of the interphase heat transfer parameter H. The figure demonstrates that increasing the interphase heat transfer parameter (H) shifts the neutral stability curves upward, raising both the critical Rayleigh number (R_{ac}) and the critical wave number (a_c). This upward shift shows that stronger thermal coupling between the fluid and solid phases exerts a stabilizing effect, requiring a greater thermal driving force to initiate convection compared to weaker heat transfer regimes.

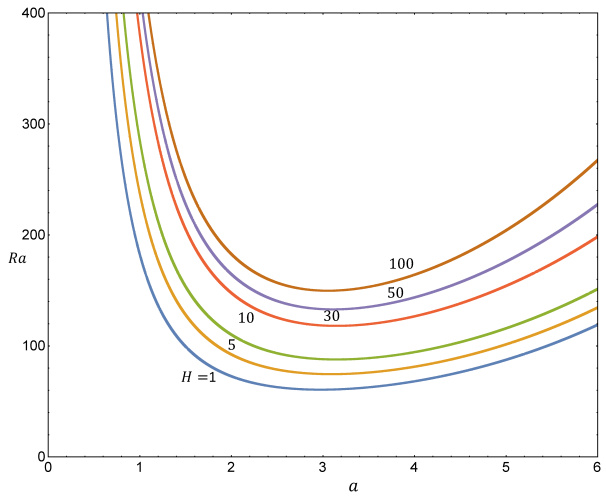


Figure 6. *Variation of Ra with wave number for different values of H.*

Figure 7 illustrates the variation of the neutral stability curves with the wave number for different values of the conductivity ratio (γ). We observe that increasing the conductivity ratio (γ) decreases the critical Rayleigh number, exerting a destabilizing effect, whereas decreasing the ratio enhances system stability. Furthermore, shifts in the minimum points of the curves indicate that changes in γ alter the characteristic size of the emerging convective structures.

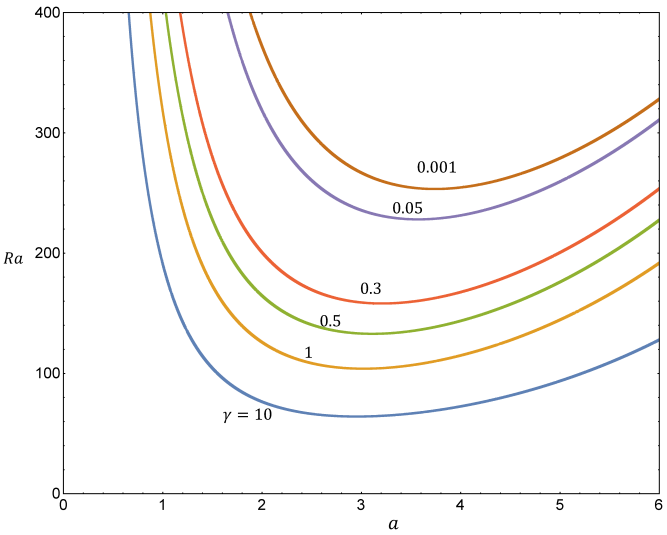


Figure 7. *Variation of Ra with wave number for different values of γ.*

Figure 8 represents the variation of neutral stability graph illustrates the variation of the Rayleigh number (Rac) against the wave number (a) for various values of the Darcy number (Da) in an anisotropic Brinkman convection system with temperature-dependent internal heat generation. In this stability framework, the region situated below each neutral curve denotes a stable state where heat is transferred purely by conduction, while the region above represents an unstable state where thermal buoyancy overcomes viscous resistance to trigger convective motion. The minimum point of each curve defines the critical Rayleigh number (Rac) and the critical wave number (ac), marking the threshold and preferred scale for the onset of convection. As the Darcy number increases from 0.01 to 20, the stability curves shift markedly upward, demonstrating that increasing Da has a strong stabilizing effect on the system. Higher Darcy numbers increase effective macroscopic viscous drag (Brinkman friction), which suppresses fluid flow and requires a much higher thermal buoyancy force (Rac) to initiate instability. Furthermore, the minimum points of the curves shift toward higher wave numbers (a) as Da increases, indicating that the resulting convective cells become progressively narrower and smaller in scale.

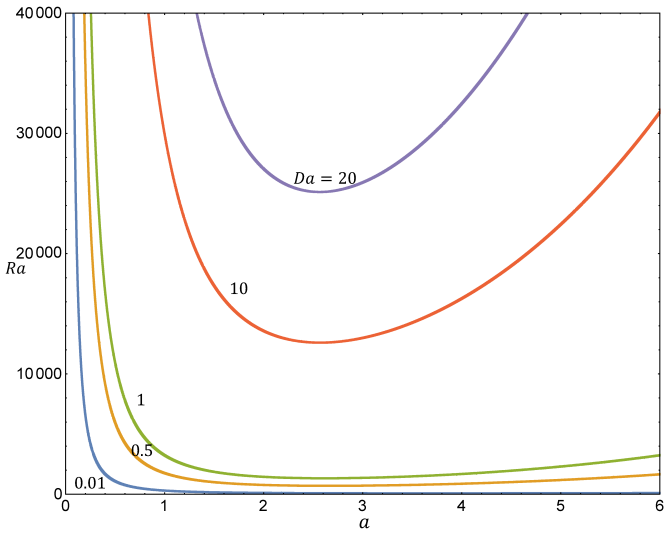


Figure 8. *Variation of Ra with wave number for different values of Da.*

Figure 9 shows the variation of critical Rayleigh number for different values of the fluid phase thermal anisotropy parameter. it is observed that the critical Rayleigh number (R_{ac}) increases with the interphase heat transfer parameter (H), exerting a stabilizing effect that requires a higher thermal driving force. For small values of H, R_{ac} remains nearly constant, whereas at high values, the curves converge toward a common asymptotic limit as strong thermal coupling drives the system near thermal equilibrium, rendering further increases in H and the effects of thermal anisotropy negligible.

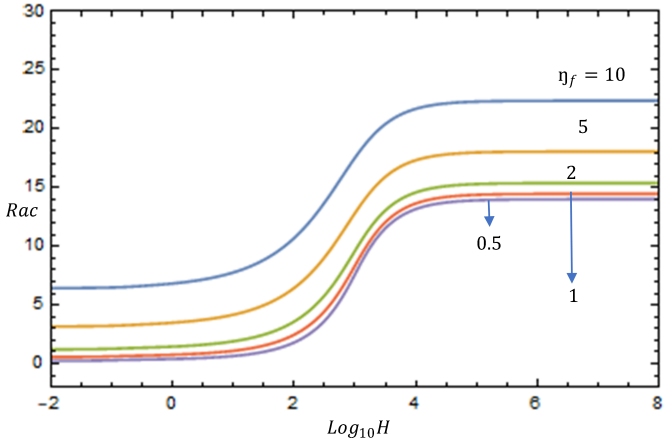


Figure 9. *Variation of Rac vs H for different values of ηf.*

Figure 10 shows that interphase heat transfer (H) and mechanical anisotropy (ξ) exert competing influences on the critical Rayleigh number (R_{ac}). Specifically, a higher interphase heat transfer parameter increases R_{ac}, creating a stabilizing effect that strengthens thermal coupling and requires a greater thermal driving force to initiate convection. Conversely, increasing the mechanical anisotropy parameter decreases R_{ac}, exerting a destabilizing effect that promotes convection at a lower thermal driving force due to altered directional permeability.

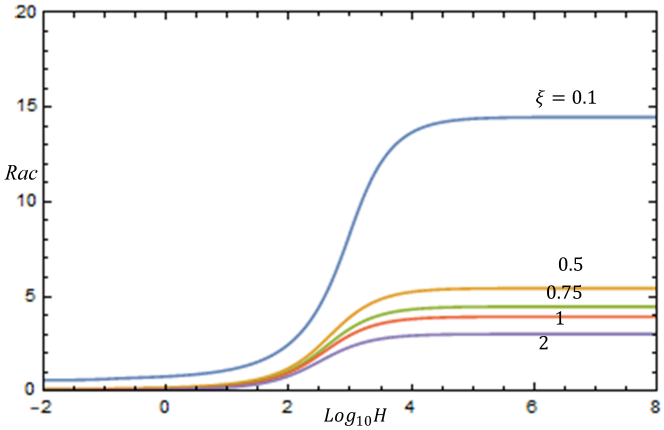


Figure 10. *Variation of Rac vs H for different values of ξ.*

Figure 11 shows that the critical Rayleigh number (R_{ac}) responds non-monotonically to the interphase heat transfer parameter (H), initially decreasing at small H before rising due to enhanced thermal coupling. Furthermore, increasing the solid-phase internal heat generation parameter raises R_{ac}, thereby delaying the onset of convection. While small H values show sensitivity to internal heating, large H drives the system toward an LTE-like limit with distinct asymptotes, demonstrating that internal heat generation persistently influences stability even under strong thermal coupling.

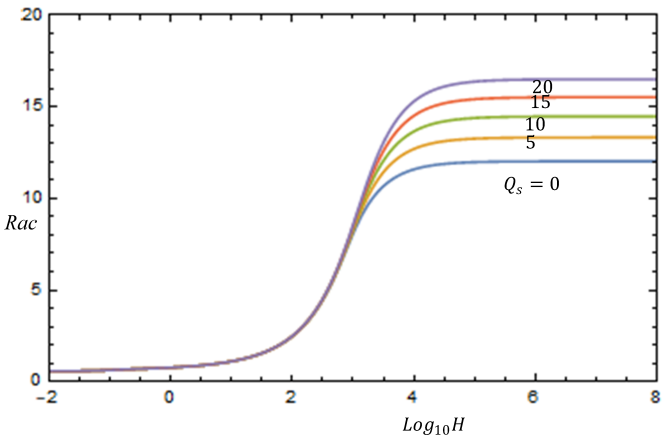


Figure 11. *Variation of Rac vs H for different values of Qs.*

Figure 12 shows that increasing the fluid-phase internal heat generation parameter raises the critical Rayleigh number (R_{ac}),

exerting a stabilizing effect that delays the onset of convection. While weak interphase heat transfer (H) allows the phases to maintain separate temperature profiles, large H values enhance thermal coupling and drive the system toward a local thermal equilibrium (LTE)-like state with distinct asymptotic limits. Although qualitatively similar to solid-phase internal heat generation, fluid-phase heating operates through distinct energy equations to shape system stability.

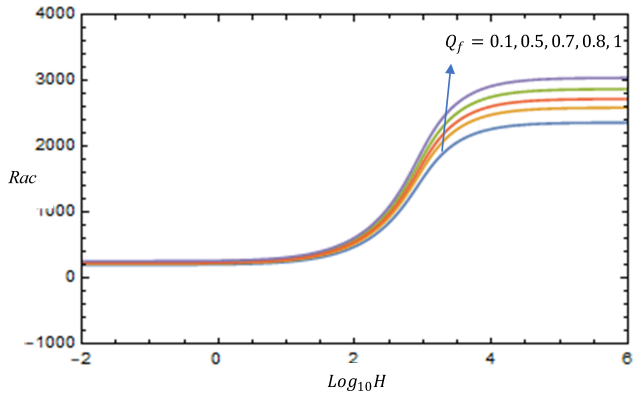


Figure 12. *Variation of Rac vs H for different values of Q f.*

Figure 13 shows the variation of the critical Rayleigh number with H for different values of conductivity ratio (γ). The figure demonstrates that the conductivity ratio (γ) has a negligible effect on system stability at low interphase heat transfer (H), but its influence grows significantly as H increases. Specifically, decreasing γ reduces the critical Rayleigh number (R_{ac}), exerting a destabilizing effect that requires a lower thermal driving force to trigger convection, while simultaneously decreasing the critical wave number (a_c) to enlarge the horizontal scale of convective cells.

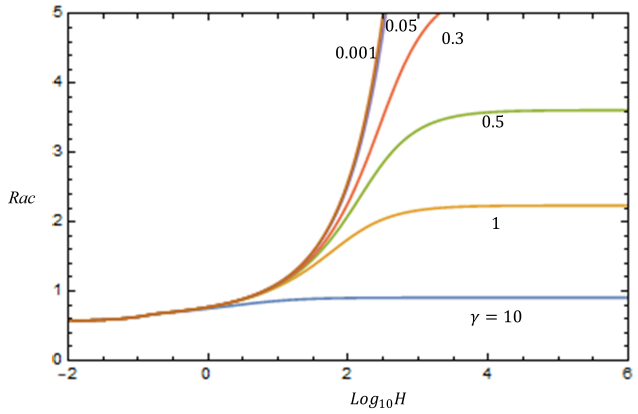


Figure 13. *Variation of Rac vs H for different values of γ.*

Figure 14 shows the variation of critical Rayleigh number with H for different values of solid-phase thermal anisotropy ns. It is observed that at very low interphase heat transfer (H), the critical Rayleigh number (R_{ac}) is nearly independent of the solid-phase thermal anisotropy parameter (ns), with convection being primarily fluid-governed. As H increases, the curves diverge, revealing that both higher H and increased ns raise R_{ac} and exert a stabilizing effect. This demonstrates that stronger thermal coupling allows solid-phase thermal anisotropy to increasingly delay the onset of convection by modifying heat redistribution within the porous matrix.

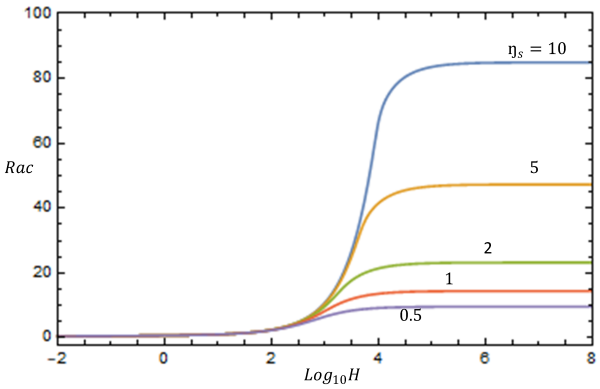


Figure 14. *Variation of Rac vs H for different values ηs.*

Figure 15 shows the variation of critical wave number with H for different values of solid-phase internal heat generation. Figure shows a non-monotonic relationship between the critical wave number and the interphase heat-transfer coefficient (H) across varying solid-phase internal heat generation values. At small H, curves are closely spaced and increase gradually; in the intermediate range, they rise to a peak (reaching ≈ 3.19) before declining. At high H, all curves converge to a common limiting value (≈ 2.95) as strong thermal coupling drives the system toward local thermal equilibrium.

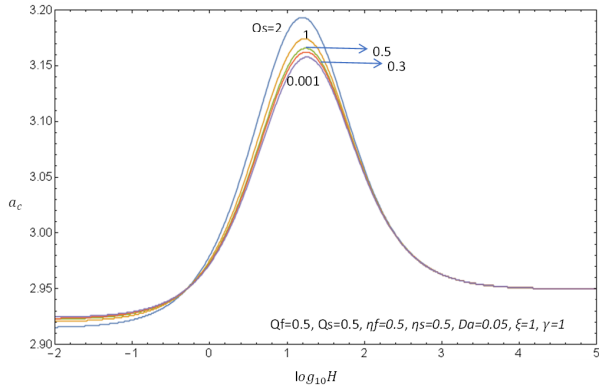


Figure 15. *Variation of 'a' Vs H for different values of Qs.*

Figure 16 shows the variation of critial wave number with H for different values of conductivity ratio (γ). It is observed that the conductivity ratio (γ) has a negligible effect on the critical wave number (R_{ac}) at low interphase heat transfer (H). As H increases, however, the curves diverge: decreasing γ reduces a_c, exerting a destabilizing effect that requires a lower thermal driving force, while also lowering the critical wave number (a_c) to enlarge the horizontal scale of convective cells.

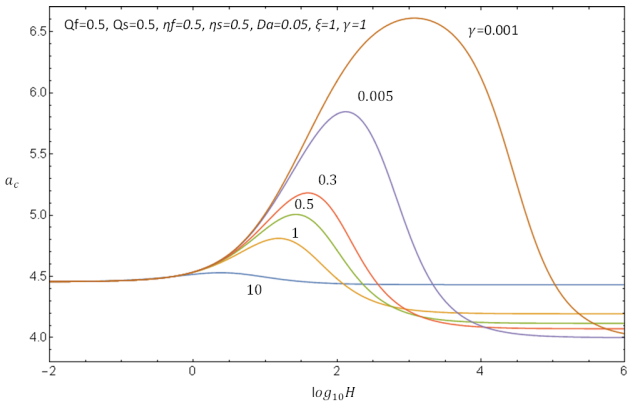


Figure 16. *Variation of 'a' Vs H for different values of* γ.

Figure 17 illustrates the variation of the critical wave number with the interphase heat-transfer coefficient H for different values of the fluid-phase thermal anisotropy parameter, while other parameters are fixed. It is observed that for very small values of H, the curves are distinct, indicating that the effect of thermal anisotropy is significant when there is slow transfer of heat between the phases, which again shows that the thermal anisotropy parameter has a strong effect in the weak interphase heat-transfer regime.

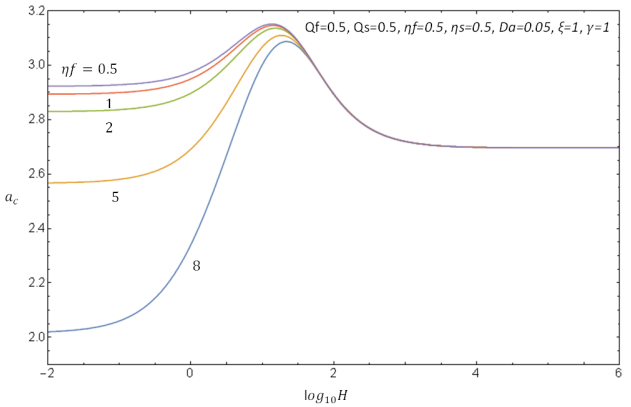


Figure 17. *Variation of 'a' Vs H for different values of* ηf.

Figure 18 illustrates the variation of the critical wave number a_c with the interphase heat transfer coefficient for different values of the fluid-phase internal heat generation parameter Q_f under thermal non-equilibrium conditions. At low interphase heat transfer rates ($\log_{10} H < 0$), the curves are well-separated, where lower Q_f values yield higher initial critical wave numbers (e.g., $a_c \approx 2.95$ for $Q_f = 0.001$) compared to larger Q_f values (e.g., $a_c \approx 2.83$ for $Q_f = 2$). As $\log_{10} H$ increases, the critical wave number for all curves rises sharply to a peak exceeding 3.15 around $\log_{10} H \approx 1.3$, subsequently declining and converging into a single horizontal asymptote at approximately $a_c \approx 2.95$ for $\log_{10} H > 4$. This behavior indicates that variations in fluid-phase internal heat generation significantly influence convective cell sizes in the low-to-moderate heat transfer regime, whereas their influence is entirely neutralized at high interphase heat transfer values as the system approaches thermal equilibrium.

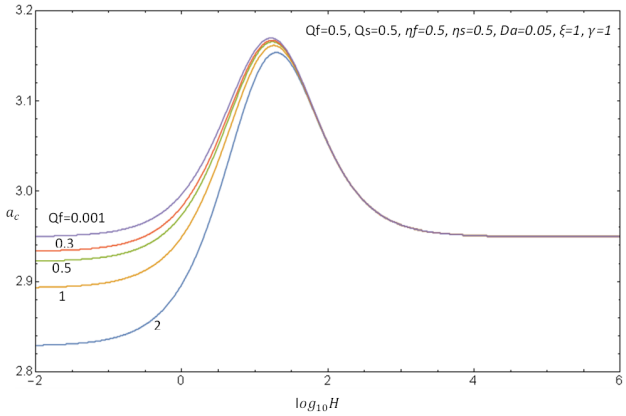


Figure 18. *Variation of 'a' Vs H for different values of* Qf.

Figure 19 shows the variation of critical wave number with H for different values of the solid-phase thermal anisotropy parameter. The figure illustrates that system stability and critical wave numbers (a_c) are heavily influenced by the interphase heat transfer coefficient (H) and the solid-phase thermal anisotropy parameter ns across three distinct regimes. At low heat transfer ($\log_{10} H < 0$), all curves converge at $a_c \approx 2.92$ independently of η_s, indicating a fluid-governed regime where convection occurs under a small thermal driving force. As heat transfer increases to the moderate regime ($\log_{10} H \approx 1.5$), a_c peaks above 3.3, and higher values of both H and ns raise the critical Rayleigh number, exerting a stabilizing effect that delays the onset of convection. Finally, in the high heat transfer regime ($\log_{10} H > 4$), the curves diverge into distinct asymptotic limits—such as $a_c \approx 2.95$ for ns = 0.5 compared to 1.82 for ns = 8, demonstrating that solid-phase thermal anisotropy crucially dictates convective cell structures and final stability states.

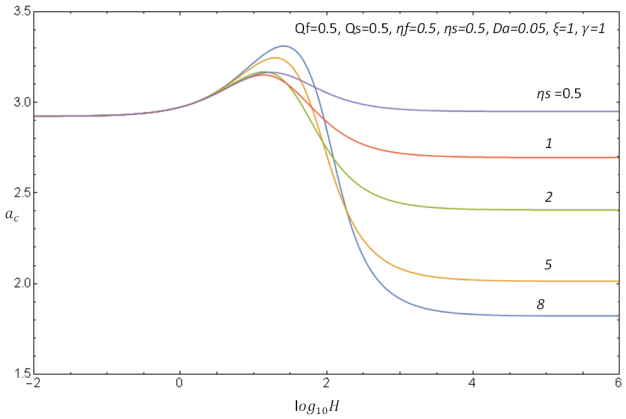


Figure 19. *Variation of 'a' Vs H for different values of η.*

Figure 20 shows the variation of critical wave number for different values of mechanical anisotropy parameter (ξ). Here we see that as $\log_{10} H$ increases to moderate levels ($\sim$ 1.3 to 1.5), the critical wave number (a_c) rises to a peak before leveling off into distinct horizontal asymptotes at high heat transfer ($\log_{10} H > 4$). Specifically, lower values of ξ and higher values of Da yield significantly higher critical wave numbers, demonstrating that both parameters persistently dictate convective cell structures across all regimes without converging to a single unified limit.

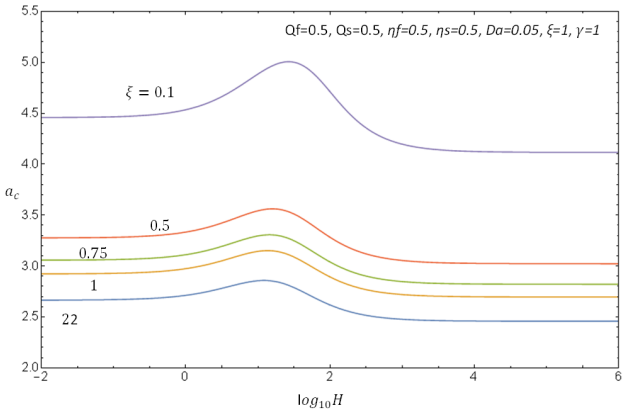


Figure 20. *Variation of 'a' Vs H for different values of ξ.*

4. Conclusion

The onset of thermal convection in an anisotropic, fluid-saturated porous layer with temperature-dependent internal heat generation has been investigated using the local thermal non-equilibrium (LTNE) model. The effects of mechanical anisotropy, fluid-phase and solid-phase thermal anisotropy, conductivity ratio, interphase heat transfer, and phase-specific internal heat generation on the stability characteristics of the system have been examined through the neutral stability curves and the variation of the critical Rayleigh number. The principal conclusions drawn from the present investigation are summarized as follows.

Neutral stability characteristics: The neutral stability curves exhibit distinct minimum points corresponding to the critical Rayleigh number and critical wave number. These important quantities determine the threshold for the onset of convection and the characteristic horizontal scale of the convective cells. An increase of the critical Rayleigh number makes the system more stable; a decrease allows convection to be initiated by a smaller thermal driving force.

Effect of solid-phase thermal anisotropy: The solid-phase thermal anisotropy parameter significantly influences the onset of convection. The critical Rayleigh number increases with increasing solid-phase thermal anisotropy over the parameter ranges considered, indicating a stabilizing effect. This influence becomes more pronounced when the interphase heat transfer parameter is sufficiently large, while the critical Rayleigh number remains relatively insensitive to solid-phase thermal anisotropy at very low interphase heat transfer rates.

Effect of ratio of conductivities: The ratio of the conductivities plays a role in the stability of the system by modifying the relative thermal transport properties of the fluid and solid phases. Its effect on the critical Rayleigh number is relatively weak at small values of the interphase heat transfer parameter. As interphase heat transfer increases, the stability curves become more sensitive to changes in the conductivity ratio. Within the parameter range examined, decreasing the conductivity ratio reduces the critical Rayleigh number, as indicated by the numerical results, thereby promoting the onset of convection.

Effect of fluid-phase thermal anisotropy: The fluid-phase thermal anisotropy parameter has a significant influence on the critical conditions for convection. The reported results indicate that its effect may depend on the parameter range: an increase in the critical Rayleigh number corresponds to enhanced stability, whereas a decrease indicates a destabilizing influence. This behaviour highlights the importance of directional thermal conduction in determining the temperature distribution and the onset of buoyancy-driven motion in the porous layer.

Interphase heat transfer effect: The interphase heat transfer parameter is very important in controlling the thermal interaction between the fluid and solid phases. For the parameter ranges in which the critical Rayleigh number increases with interphase heat transfer, stronger thermal coupling delays the onset of convection and stabilizes the system. At sufficiently large values of the interphase heat transfer parameter, the critical Rayleigh number approaches an asymptotic limit, indicating

that further increases in thermal coupling have a diminishing influence on the stability threshold.

Effect of mechanical anisotropy: The mechanical anisotropy parameter has a destabilising effect in the range considered, as shown by the decrease in the critical Rayleigh number with increasing mechanical anisotropy. This behaviour suggests that variations in the directional permeability properties of the porous matrix can decrease the resistance to buoyancy-driven flow and promote the onset of convection. Its physical meaning is exactly given by the definition of the mechanical anisotropy parameter that is used in the governing equations.

Effect of solid-phase internal heat generation: The solid-phase internal heat generation parameter influences the stability threshold by modifying the thermal field within the porous matrix. The reported increase in the critical Rayleigh number with this parameter indicates a stabilizing effect over the investigated range. The dependence of the critical Rayleigh number on the interphase heat transfer parameter further demonstrates that the influence of solid-phase heating is closely associated with the strength of thermal coupling between the two phases.

Effect of fluid-phase internal heat generation: The fluid-phase internal heat generation parameter also affects the onset of convection. The critical Rayleigh number increases with this parameter over the range considered, indicating a delay in the onset of convective instability. The trends observed at small and large values of the interphase heat transfer parameter are qualitatively similar to those associated with solid-phase internal heat generation, although the magnitude of their effects may differ because the two heat sources enter separate energy equations.

Combined influence of thermal parameters: The results demonstrate that the stability of the porous layer is governed by the combined effects of thermal anisotropy, conductivity ratio, interphase heat transfer, and internal heat generation in both phases. The influence of an individual parameter cannot always be interpreted independently, since changes in thermal coupling can alter the sensitivity of the critical Rayleigh number to the other parameters.

Limiting behaviour and physical significance: At sufficiently large interphase heat transfer rates, the fluid and solid phases tend towards thermal equilibrium, and the LTNE system approaches a local thermal equilibrium (LTE)-like limit. The limiting critical Rayleigh numbers depend on the remaining governing parameters, including the phase-specific internal heat generation terms. This asymptotic behaviour provides insight into the transition from weak to strong thermal coupling in anisotropic porous media.

Finally, the present study demonstrates that the onset of convection in an anisotropic porous medium with temperature-dependent internal heat generation is strongly influenced by the interaction of mechanical properties, directional thermal transport, interphase heat exchange, and phase-specific heating. The results provide a framework for understanding how these parameters modify the critical conditions for convective instability and may be useful in the analysis and design of porous systems involving coupled heat transfer and internal energy generation.

Abbreviations

k_f	Thermal Conductivity Tensor of the Fluid Phase
k_s	Thermal Conductivity Tensor of the Solid Phase
(x, y, z)	Space Coordinates
H	Inter-Phase Heat Transfer Coefficient
κ_f	Thermal Diffusivity
Q_f	Internal Heat Generator for Fluid Phase
Q_s	Internal Heat Generator for Solid Phase
RA	Rayleigh Number, $\frac{\rho_0 g\beta h\left((T_f - T_u)K_z\right)}{\epsilon\mu_f\kappa_f}$
K	Permeability Tensor, $K_h(ii + jj) + K_z kk$
T	Temperature
a	Horizontal Wave Number, $\sqrt{l^2 + m^2}$
c	Specific Heat
h	Height of the Porous Layer
g	Gravitational Acceleration
l, m	Wave Numbers in the x and y Directions Respectively
p	Pressure
q	Velocity Vector, (u, v, w)
t	Time
α	Diffusive Ratio
β	Coefficient of Thermal Expansion
γ	Porosity-Modified Conductivity Ratio, $\frac{\epsilon k_f}{(1-\epsilon)K}$
ϵ	Porosity
μ_f	Fluid Viscosity
θ	Dimensionless Temperature for Fluid Phase
ρ	Fluid Density
ϕ	Nondimensional Temperature of Solid Phase
ω	Growth Rate
∇_1^2	$\frac{\partial^2}{\partial x^2} + \frac{\partial^2}{\partial y^2}$
∇^2	$\nabla_1^2 + \frac{\partial^2}{\partial z^2}$
$*$	Dimensionless Quantity
$'$	Perturbed Quantity
u	Reference
f	Fluid Phase
l	Lower
s	Solid

Author Contributions

Sridhar Kulkarni: Conceptualization, Data curation, Formal Analysis, Investigation, Methodology, Software, Visualization, Validation, Writing – original draft

Nagappa Enagi: Funding acquisition, Project administration, Resources, Supervision, Writing – review & editing

Conflicts of Interest

The authors declare that they have no known financial, commercial, or personal relationships that could have appeared to influence the work reported in this paper.

Appendix

Table 1. Comparison of Ra_c and a_c for $\gamma = 1.0$ and $\gamma = 0.01$.

$\log_{10} H$	For the present case		As obtained by Banu & Rees (2002)	
	Ra_c	a_c	Ra_c	a_c
gamma = 1.0				
-2	39.502492	3.11059	39.498405	3.142388
-1.5	39.546078	3.11059	39.541537	3.144098
-1.0	39.680897	3.18014	39.677163	3.149441
-0.5	40.099392	3.18014	40.098560	3.165691
0	41.366025	3.18014	41.362100	3.211317
0.5	44.804798	3.31926	44.804663	3.313460
1.0	52.361629	3.45838	52.359639	3.436346
gamma = 0.01				
-2	39.502502	3.11059	39.498415	3.142388
-1.5	39.546180	3.11059	39.541637	3.144106
-1.0	39.681871	3.18014	39.678155	3.149520
-0.5	40.109027	3.18014	40.108280	3.166453
0	41.457251	3.2497	41.453330	3.218239
0.5	45.576683	3.38882	45.574790	3.366995
1.0	57.675518	3.73661	57.675516	3.737411

References

[1] N. Banu, D. A. S. Rees, "Onset of Darcy–Benard convection using a thermal non-equilibrium model," Int. J. Heat Mass Transfer, vol. 45, pp. 2221–2228, 2002. https://doi.org/10.1016/S0017-9310(01)00331-3

[2] K. Govender, "On the effect of anisotropy on the stability of convection in rotating porous media," Transp. Porous Med., vol. 64, no. 3, pp. 413–422, 2006. https://doi.org/10.1007/s11242-005-5479-7

[3] M. S. Malashetty, I. S. Shivakumara, and K. Sridhar, "The onset of Lapwood–Brinkman convection using a thermal non-equilibrium model," Int. J. Heat Mass Transfer, vol. 48, pp. 1155–1163, 2005.

[4] M. S. Malashetty, I. S. Shivakumara, and K. Sridhar, "The onset of convection in an anisotropic porous layer using a thermal non-equilibrium model," Transp. Porous Med., vol. 60, no. 3, pp. 199–215, 2005.

[5] A. Postelnicu, "Effect of inertia on the onset of mixed convection in a porous layer using a thermal nonequilibrium model," J. Porous Media, vol. 10, no. 5, pp. 515–524, 2007. https://doi.org/10.1615/JPorMedia.v10.i5.80

[6] R. Shivakumara and H. Mamatha, "Local thermal non-equilibrium effects on thermal convection in a rotating anisotropic porous layer," Applied Mathematics and Computation, vol. 259, pp. 838–857, 2013. https://doi.org/10.1016/j.amc.2015.03.023

[7] Amit Mahajan and Reena Nandal, "Anisotropic porous penetrative convection for a local thermal non-equilibrium model with Brinkman effects," International Journal of Heat and Mass Transfer, 2017. https://doi.org/10.1016/j.ijheatmasstransfer.2017.08.034

[8] B. Storesletten and D. Rees, "Onset of convection in an inclined anisotropic porous layer with internal heat generation," Fluids, vol. 4, no. 2, art. 75, 2019. https://doi.org/10.3390/fluids4020075

[9] Straughan, "Global nonlinear stability in porous convection with a thermal non-equilibrium model," Proceedings of the Royal Society A, vol. 462, no. 2066, pp. 409–418, 2005. https://doi.org/10.1098/rspa.2005.1555

[10] R. Nandal, "The onset of anisotropic Darcy–Brinkman penetrative convection with local thermal nonequilibrium due to heat generation and extraction," Heat Transfer, vol. 53, no. 3, pp. 1095–1116, 2024. https://doi.org/10.1002/htj.22986

[11] S. Bixapathi and A. B. Babu, "Internal heat modulation effect on convective instability in a porous layer with a magnetic field: Brinkman model," International Communications in Heat and Mass Transfer, 2026. https://doi.org/10.1016/j.icheatmasstransfer.2026.112260

[12] N. K. Enagi, K. B. Chavaraddi, and S. Kulkarni, "Couple-stress fluid saturated rotating porous layer with internal heat generation and density maximum," [Helion D journal], vol. 35, pp. 1–19, 2023. https://doi.org/10.17654/0973576323039

[13] M. Mahantesh, S. Swamy, and B. N. Hanumagowda, "Darcy–Benard–Oldroyd convection in anisotropic porous layer subject to internal heat generation," Frontiers in Materials, vol. 10, 2023. https://doi.org/10.3389/fmats.2023.1158644

[14] B. Praveena, S. Bixapathi, and A. B. Babu, "Stability of thermal convection in couple stress liquid saturated porous slab in the presence of internal heating," Physics of Fluids, vol. 37, art. 044104, 2025. https://doi.org/10.1063/5.0267176

[15] A. Nouri-Borujerdi, A. R. Noghrehabadi, and D. A. S. Rees, "Onset of convection in a horizontal porous channel with uniform heat generation using a thermal nonequilibrium model," Transp. Porous Med., vol. 69, pp. 343–357, 2007. https://doi.org/10.1007/s11242-006-9076-1

[16] G. Y. Honnappa, "Oscillatory convection in Oldroyd-B fluid-saturated porous layers under variable gravity and temperature-dependent internal heating," Heat Transfer, 2025. https://doi.org/10.1002/htj.70144

[17] G. Castinel and M. Combarnous, "Critere d'apparition de la convection naturelle dans une couche poreuse anisotrope horizontal," C. R. Acad. Sci., vol. 278, pp. 701–704, 1974.

[18] J. F. Epherre, "Critere d'apparition de la convection naturelle dans une couche poreuse anisotrope," Revue Gen. Thermique, vol. 168, pp. 949–950, 1975.

[19] D. B. Ingham and I. Pop (eds.), Transport Phenomena in Porous Media, Pergamon, Oxford, 1998.

[20] A. Khalili, I. S. Shivakumara, and M. Huettel, "Effects of throughflow and internal heat generation on convective instabilities in an anisotropic porous layer," J. Porous Media, vol. 5, pp. 187–198, 2002.

[21] A. V. Kuznetsov, "Thermal non-equilibrium forced convection in porous media," in Transport Phenomena in Porous Media, D. B. Ingham and I. Pop (eds.), Pergamon, Oxford, pp. 103–130, 1998.

[22] O. Kvernvold and P. A. Tyvand, "Nonlinear thermal convection in anisotropic porous media," J. Fluid Mech., vol. 90, pp. 609–624, 1979.

[23] R. McKibbin, "Thermal convection in a porous layer: effects of anisotropy and surface boundary conditions," *Transp. Porous Media*, vol. 1, pp. 271–292, 1986.

[24] item D. A. Nield and A. Bejan, *Convection in Porous Media*, 2nd ed., Springer-Verlag, New York, 1999.

[25] T. Nilsen and L. Storesletten, "An analytical study of natural convection in isotropic and anisotropic porous channels," *Trans. ASME J. Heat Transfer*, vol. 112, pp. 396–401, 1990. https://doi.org/10.1115/1.2910390

[26] Y. Qin and P. N. Kaloni, "Convective instabilities in anisotropic porous media," *Studies in Applied Mathematics*, vol. 91, pp. 189–204, 1994.

[27] D. A. S. Rees and I. Pop, "Free convective stagnation point flow in a porous medium using thermal non-equilibrium model," *Int. Commun. Heat Mass Transfer*, vol. 26, pp. 945–954, 1999. https://doi.org/10.1016/S0735-1933(99)00084-6

[28] D. A. S. Rees and I. Pop, "Vertical free convective boundary layer flow in a porous medium using a thermal nonequilibrium model," *J. Porous Media*, vol. 3, pp. 31–44, 2000. https://doi.org/10.1615/JPorMedia.v3.i1.30

[29] D. A. S. Rees and I. Pop, "Vertical free convective boundary layer flow in a porous medium using a thermal nonequilibrium model: elliptic effects," *J. Appl. Math. Phys.*, vol. 53, pp. 1–12, 2002.

[30] L. Storesletten, "Effects of anisotropy on convective flow through porous media," in *Transport Phenomena in Porous Media*, D. B. Ingham and I. Pop (eds.), Pergamon Press, Oxford, pp. 261–283, 1998.

[31] P. A. Tyvand and L. Storesletten, "Onset of convection in an anisotropic porous medium with oblique principal axes," *J. Fluid Mech.*, vol. 226, pp. 371–382, 1991. https://doi.org/10.1017/S0022112091002422

[32] K. Vafai (ed.), *Handbook of Porous Media*, Marcel Dekker, New York, 2000.